THE JOURNAL OF PHYSICAL CHEMISTRY B

Subscriber access provided by University of South Dakota

B: Fluid Interfaces, Colloids, Polymers, Soft Matter, Surfactants, and Glassy Materials

Rational Design of a Famotidine-Ibuprofen Co-Amorphous System: An Experimental and Theoretical Study

marcos guillermo Russo, Hector Armando Baldoni, Yamina A. Dávila, Elena Virginia Brusau, Javier A. Ellena, and Griselda E. Narda

J. Phys. Chem. B, **Just Accepted Manuscript** • DOI: 10.1021/acs.jpcb.8b06105 • Publication Date (Web): 30 Aug 2018

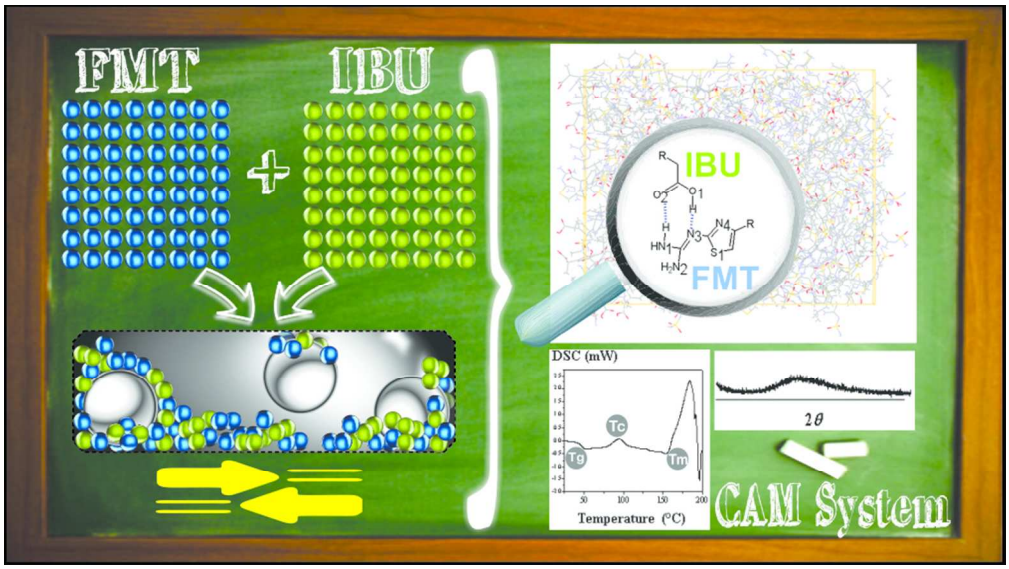

85x47mm (300 x 300 DPI)

Rational Design of a Famotidine-Ibuprofen Co-amorphous System: An Experimental and Theoretical Study

Marcos G. Russo*,[†, ‡]; Hector A. Baldoni.[†,§]; Yamina A. Dávila[†, ‡]; Elena V. Brusau[†,‡]; Javier A. Ellena[‖]; Griselda E. Narda*[†,‡]

† Departamento de Química. Facultad de Química, Bioquímica y Farmacia. Universidad Nacional de San Luis. Chacabuco 917. D5700HOJ San Luis, Argentina.

‡ Instituto de Investigación en Tecnología Química (INTEQUI-UNSL), CONICET, Almirante Brown 1455. D5700HGC San Luis, Argentina.

§ Instituto de Matemática Aplicada San Luis (IMASL-UNSL), CONICET. Italia 1556, D5700HHW San Luis, Argentina.

‖Instituto de Fisica de São Carlos, Universidad de São Paulo, CP 369, 13560-970 São Carlos, SP, Brazil.

ABSTRACT

Famotidine (FMT) and ibuprofen (IBU) were used as model drugs to obtain co-amorphous systems, where the guanidine moiety of the antacid and the carboxylic group of the NSAID, could potentially participate in H-bonds leading to a given structural motif. The systems were prepared in 3:7, 1:1 and 7:3 FMT and IBU molar ratios, respectively. The latter two became amorphous after 180 minutes of co-milling. 1:1 FMT-IBU exhibited a higher physical stability in assays at 4, 25 and 40 °C up to 60 days. FTIR spectroscopy accounted for important modifications in the vibrational behavior of those functional groups, allowing to ascribe the skill of 1:1 FMT-IBU for remaining amorphous to equimolar interactions between both components. DFT calculations followed by QTAIM analysis were then conducted to support the presence of the expected FMT-IBU heterodimer with consequently formation of a $R_2^2 8$ structural motif. The electron density (ρ) and its Laplacian ($\nabla^2\rho$) values suggested a high strength of the specific intermolecular interactions. Molecular Dynamics simulations to build an amorphous assembly, followed by RDF analysis on the modeled phase were further employed. The results demonstrate that is feasible a rational design of a co-amorphous system, satisfactorily stabilized by molecular-level interactions leading to the expected motif.

1. INTRODUCTION

The major issue of orally administered marketed drugs is currently their limited water solubility. Grohganz *et al.*[1] and Rumondor *et al.*[2] reported that more than 90% of new candidates to reach the market shows poor aqueous solubility. Several formulation strategies have been used to overcome this problem: reduction of the particle size

(nano-drug delivery),[3] preparation of salts, cocrystals (i.e. crystal engineering)[4,5] or inclusion complexes,[6] or the use of lipid based vehicles.[7] In addition to these alternatives, the obtainment of amorphous phases of active pharmaceutically ingredients (APIs) is a potent tool to improve pharmacokinetic parameters such as solubility and intrinsic dissolution rate[8]. In this sense, two techniques have been broadly explored: the solid dispersion technology[9] and, the obtainment of co-amorphous (CAM) phases – so called co-amorphous formulations– consisting of two low molecular weight molecules in stoichiometric ratios that stabilize each other in the amorphous form.[10] However, the CAM phases are preferred over the formulations obtained by the solid dispersion method due to a series of advantages, such as *i*: do not show procedural disadvantages like hygroscopicity, that reduces the glass transition temperature (T_g) leading to phase separation and further recrystallization; in addition, due to the limited miscibility of some drugs in the polymer, large quantities of polymer for an appropriate drug loading are required, and *ii*: higher physical stability, solubility and increased intrinsic dissolution velocity.[11] It is noteworthy that co-administration of two APIs, as an amorphous powder in a single formulation, provides compliance-related benefits since it implies simplicity for the patient and fewer administrations that ensure a more efficient treatment. Therapeutic advantages can also be achieved by a convenient combination of drugs where for example, one prevents the side effects of the other. The improvement in the physicochemical properties is mainly attributed to the new intermolecular interactions between the components of the system. Moreover, the lower molecular mobility of CAM phases and consequently, their lesser ability to nuclear and recrystallize respecting monocomponent amorphous forms, is also ascribed to these interactions.[12] In spite of the relevance of such interactions in CAM systems (CAMs), they still play a secondary role in the study of these phases. This

observation is mainly attributed to the fact that several works are focused on the synthesis and further study of the presence or absence of intermolecular interactions,[13,14,15] without taking into account their importance. The first works dealing with rationalized intermolecular interactions in CAMs involved a drug and an amino acid as excipient.[16,17,18,19,20,21] Such studies were based on the assumption that if APIs interact at the molecular level with the target sites of their respective receptor proteins, they also may able to interact with amino acids in CAM. Recently, Korhonen *et al.*[22] reported a study with a coherent selection of excipients, concluding that no preliminary rational design for the synthesis of CAM phases can ensure the physical stability of these systems.

Although the amorphous state does not show a long range tridimensional order, the formation of heterodimers in CAMs is already reported by Löbmann, K. *et al.* where it was suggested that naproxen and indomethacin stabilize through O-H···O forming a $R_2^2 8$ structural motif involving the complementary carboxylic moieties of both drugs.[23,24] In addition, the presence of heterotrimers was also proposed in CAM solids. Dengale *et al.*[25] proposed that ritonavir and quercetin form heterotrimers possibly by O-H···O intermolecular interactions. Both CAMs fulfill the rule formulated by Etter for H-bond interactions,[26,27] which establishes that for a multifunctional system, the best donor atom in a given molecule preferentially interacts with the best acceptor belonging to the other, whereas the second best donor-acceptor pair will interact each and so on.

In the present work, ibuprofen (IBU) and famotidine (FMT) (Figure 1A*a* and 1A*b*, respectively) were selected to prepare a CAMs to probe that a rational design, leading to a desired structural motif constructed by specific N-H···O and O-H···N intermolecular interactions, can be performed. Multiples H-bond donors and acceptors are observed in the

chemical structure of FMT, the imine nitrogen atom (N3) being the most basic[28,29] and therefore, the most appropriate to participate in H-bond interactions with a given donor group. On the other hand, the hydroxyl group (H-O1) of the carboxylic moiety is the main H-bond donor in IBU.[30] Taking into account the previous analysis and the Etter´s rule, is feasible that FMT and IBU interact through these functional group ($O1\text{-}H_{(IBU)}\cdots N3_{(FMT)}$). Moreover, the carbonyl oxygen atom of IBU could participate as H-bond acceptor with the primary amines of FMT ($N(1\text{ or }2)\text{-}H_{(FMT)}\cdots O2_{(IBU)}$). Both proposed intermolecular interactions would be able to give rise FMT-IBU heterodimers with consequent formation of a $R\,^{2}_{2}8$ structural motif (Figure 1B).

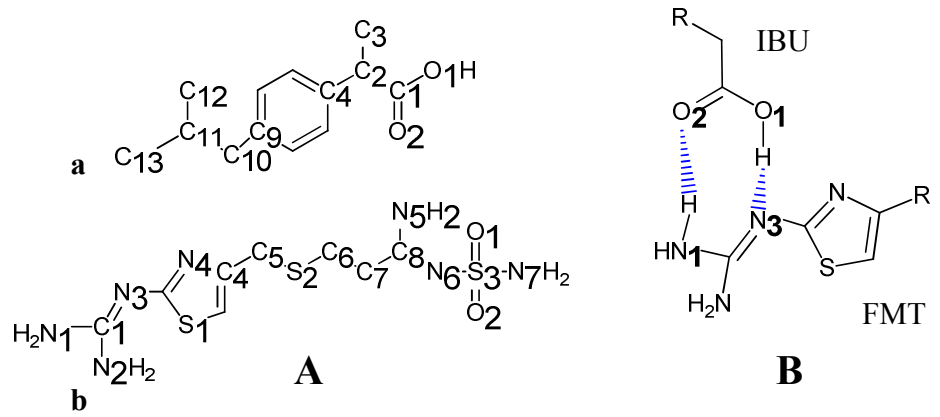

Figure 1: A) Chemical structure and atom numbering of IBU (a) and FMT (b).

B) Proposed interactions in the FMT-IBU CAMs.

The co-milling technique is a widely used method to amorphize APIs. Thus, different molar ratios of polymorph A of famotidine (A-FMT) and IBU (3:7, 1:1 and 7:3, respectively) were co-milled during several periods. The resulting binary systems were characterized by an adequate combination of solid state techniques such as DRXP, Polarized Light Thermal Microscopy, DSC and FTIR spectroscopy. Moreover, theoretical calculations were performed due to their invaluable assistance in the study of amorphous

phases where obviously, no structural information by diffraction technique is available. Then, the feasibility of formation of heterodimers FMT-IBU was evaluated by DFT calculations whereas the strength of the intermolecular interactions between the APIs was estimated by means of QTAIM analysis. Molecular Dynamics (MD) simulations on a modeled co-amorphous solid were further performed not only to study the intermolecular interactions but also the H-bonds distribution in this system by Radial Distribution Function (RDF) analysis.

2. EXPERIMENTAL SECTION

2.1. Materials

FMT (MW: 337.4 g mol^{-1}) was purchased from Fluka® as a polymorphic mixture of A and B forms (A-FMT and B-FMT, respectively) and used as received. The A-FMT, used in the binary systems preparation, was obtained as described in Hassan *et al.*[31] and tested by comparing the corresponding powder X-ray diagram and IR spectrum with those reported in the literature.[32] Raw IBU (MW: 206.29 g mol^{-1}) 97.8% was provided by the Drug Quality Control Laboratory (National University of San Luis). Its purity was determined by HPLC analysis using IBU 99.8% sourced from Sigma® as standard.

2.2. Methods

2.2.1. Preparation of amorphous phases

Amorphous ibuprofen and famotidine

Ibuprofen and famotidine did not amorphize by milling and instead their amorphous phases could be prepared by quench-cooling. IBU powder (~3 mg) was placed in an aluminum pan

with cover and melted upon heating in the differential scanning calorimeter (DSC; see description below for further instrumental details). Then, the DSC was fastly cooled to −80 °C and further heated to 150 °C at 10 ºC min^{-1}; the glass transition temperature (T_g) of the amorphous phase was detected during the second step of heating. Raw FAM (~50 mg) was taken in a silica crucible and completely melted in a hot plate. Liquid nitrogen was carefully poured upon the melted compound. Once the sample solidified, ~ 3 mg were analyzed by DSC to determine the T_g by heating up to 100 ºC.

Co-amorphous systems

The pure drugs and the binary systems at 3:7, 1:1 and 7:3 molar ratios of A-FMT and IBU, respectively, were co-milled using an oscillatory ball mill Mixer Mill MM400 RETSCH, placing 200 mg of each sample in a 25 mL volume stainless steel milling jar containing three 7 mm diameter stainless steel balls. The milling conditions were fixed at a frequency of 30 Hz during 180 minutes and the jar was immersed into liquid nitrogen each 20 minutes. The process was conducted in a room at 25 ± 2 °C. The samples were analyzed as soon as they were obtained. Physical mixtures in the same molar ratios were also prepared by mixing both APIs with a spatula in a mortar in order to perform some comparisons with the co-milled ones when was necessary.

2.2.2. X-ray powder diffraction (XRPD)

X-ray powder diffraction patterns were obtained with a Rigaku ULTIMA IV diffractometer operating at 25 ºC with CuKα radiation (Ni-filter) and NaCl and quartz as external calibration standards. The diffractograms were recorded in the 2θ angle range 3-45º and the process parameters were set at 0.02 2θ scan step size and 2s scan step time.

2.2.3. Differential Scanning Calorimetry (DSC)

DSC curves were obtained with a Shimadzu TA-60WS Thermal Analysis System using 3-5 mg of each sample in open aluminum pans with flowing air at 50 mL min^{-1} and a heating rate of 10 ºC min^{-1} from -30 to 200 ºC (Figure S1). Calibration of the DSC instrument was carried out using indium as standard. The T_g was determined as the midpoint of the change in the heat capacity of the samples, while both T_c (recrystallization temperature) and T_m (melting temperature) were determined as the onset temperatures. Each assay was performed in triplicate.

The experimental T_g values of the CAM samples were compared with the predicted T_g values from the Gordon-Taylor equation:

$$T_{g(mix)} = \frac{w_1 T_{g1} + K\, w_2\, T_{g2}}{w_1 + K\, w_2} \quad (1)$$

where $T_{g(mix)}$ is the glass transition temperature of the CAM binary system, w_1 and w_2 are weight fractions, K is a constant and T_{g1} and T_{g2} are the experimental T_g values of components 1 and 2, respectively. K was calculated as:

$$K = \frac{T_{g1}\, \rho_1}{T_{g2}\, \rho_2} \quad (2)$$

where ρ1 and ρ2 are the densities of the pure amorphous compound. In this paper, the density values employed were the corresponding to the crystalline drugs (A-FMT = 1.595 g

cm^{-3} [33] and IBU = 1.396 g cm^{-3} [34]). As it was described by Alleso, M. *et. al.*[35], this approximation is valid for small molecules such as those used in this work.[36,37]

2.2.4. Thermogravimetric Analysis (TGA)

TG curves were obtained with a Shimadzu TGA 51 thermal analyzer using platinum pans, flowing oxygen at 50 mL min^{-1} and a heating rate of 10 ºC min^{-1} from room temperature to 250 ºC.

2.2.5. Polarized Light Thermal Microscopy (PLTM)

Hot-stage microphotographs were acquired in a Linkam Hot-Stage system, model THMS600 equipped with a Leica DM2500 microscope and a Pixelink PL-A662 video camera. LINKSYS 32 DV-NC system software by Linkam, was used for temperature control, image record and analysis. The images were obtained by the combined use of polarized light and wave compensators using a 10X magnification.

2.2.6. Fourier Transform Infrared Spectroscopy

Fourier Transform Infrared (FTIR) spectra were recorded on a Nicolet PROTÉGÉ 460 spectrometer provided with a CsI beamsplitter in the 4000-400 cm^{-1} range with 64 scans and a spectral resolution of 2 cm^{-1} using the KBr pellet technique.

2.2.7. Stability studies

The amorphous co-milled binary systems (1:1 and 7:3 FMT-IBU) were stored in desiccators under dry conditions (silica gel) at 4, 25 and 40 °C up to 60 days. The physical stability was further analyzed by XRPD.

2.2.8. Computational methods

2.2.8.1. DFT calculations

Geometry optimizations without any symmetry constraints were carried out with GAUSSIAN 09[38] package at Density Functional Theory (DFT) level of theory adopting the popular B3LYP hybrid approximations for the exchange–hybrid correlation functional.[39] A standard 6-311G(d,p)[40] basis set was selected capping all the atomic centers. Stationary points were characterized by calculating the Hessian matrix analytically at this level of theory. The electronic charge distribution was also analyzed with the Quantum Theory of Atoms in Molecules (QTAIM)[41] performed with the AIMPAC program suite[42] at the refined electron density computed at the B3LYP/6-311++G(d,p)[39,40] level of theory.

2.2.8.2. Molecular Dynamics simulations

The initial geometries of A-FMT (CCDC number: 215086) and IBU (CCDC number: 1041370) were constructed from the experimental crystal structure. These geometries were transferred to AmberTools17[43] for the GAFF force field parameters[44] assignment and the RESP partial charges assigned to reproduce the electrostatic potential determined at the HF/6-31G(d) level of theory using Gaussian 09.[38] MD simulations of the amorphous FMT-IBU model system was carried out with a fixed number of 125 molecules of each drug, randomly placed in a cubic box subject to the conventional periodic boundary conditions.

First of all, the model system was energy minimized until the RMSD of the gradient components was less than 0.1 kcal $mol^{-1}Å^{-1}$. Then, constant volume and temperature (NVT) molecular dynamics, starting from a temperature of 50 K and targeting 400 K were performed; the quenched system was annealed at 400 K during 5 ns. After that, the system was cooled to a final temperature of 298 K at a cooling rate of 0.017 K ps^{-1}. This quench-and-cooling process was repeated five times starting from the geometrical coordinates generated in the previous cycle. Finally, constant pressure and temperature (NPT) production stage at 298 K was followed for 600 ns and coordinates were written every 5 ps. MD were performed by the GPU implementation of the pmemd program[45,46,47] included in the AMBER16 suite of programs.[48] The Particle Mesh Ewald method[49] was employed with a direct non-bonded cutoff of 8 Å. A timestep of 1 fs was used in all MD stages. Bonds involving hydrogen atoms were constrained with the SHAKE algorithm.[50] The temperature was controlled with the stochastic Langevin thermostat,[51] using a collision frequency of 5 ps^{-1}. Pressure was controlled with the Berendsen barostat,[52] targeting a pressure of 1 bar and using a relaxation time of 2 ps. Data for calculation of the RDF of the structure of the amorphous state was collected for the last 50 ns of production and averaged to obtain the final results. To estimate the T_g a glass was generated by fast cooling the molten system from 380 K to 150 K at a cooling rate of 0.03 K ps^{-1} starting from the last coordinates of the model system obtained at the production stage.

3. RESULTS AND DISCUSSION

3.1. SOLID STATE CHARACTERIZATION

The milling process has demonstrated to be a powerful technique for transforming a crystalline drug into its amorphous counterparts;[53] thus, it was used to convert the A-FMT and IBU binary system in CAM ones. According to the literature, the CAMs at 1:1 molar ratio are generally more stable than those in non-equimolar ratios,[35,54,55,56,57,58] probably due to the formation of dimers. Therefore, in this work the study of the 1:1 FMT-IBU was emphasized. However, the 3:7 and 7:3 FMT-IBU phases were also prepared and their physicochemical properties were compared with the corresponding ones to the 1:1 FMT-IBU. The powder X-ray patterns of the 3:7, 1:1 and 7:3 FMT-IBU at different milling times are shown in Figure 2. The characteristic halo of amorphous solids is observed in 1:1 and 7:3 FMT-IBU after 180 minutes of the cryo-milling process. However, diffraction peaks derived from A-FMT and IBU in 3:7 FMT-IBU were still present, so this system was discarded for further studies.

The milling process, in the same conditions used for the binary systems (180 minutes and 30 Hz), was also applied separately to A-FMT and IBU drugs. The XRPD patterns show broader diffractions with lower intensity compared with the non-milled ones. Moreover, a slightly shifted in the 2θ values of the milled drugs is observed due to the mechanical treatment (see Figure 3).

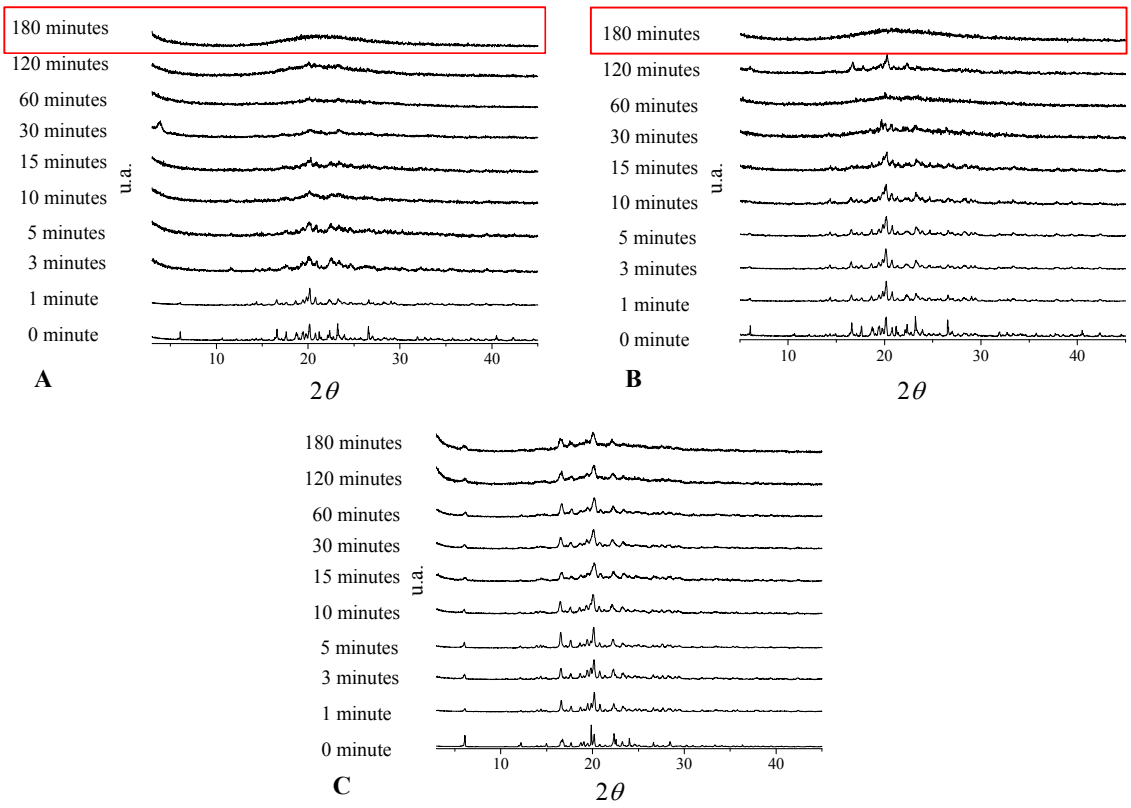

Figure 2: Powder X-ray patterns of the FMT-IBU binary systems at different milling times. A) 7:3 FMT-IBU, B) 1:1 FMT-IBU and C) 3:7 FMT-IBU. The diffractograms of FMT-IBU physical mixtures correspond to 0 minutes.

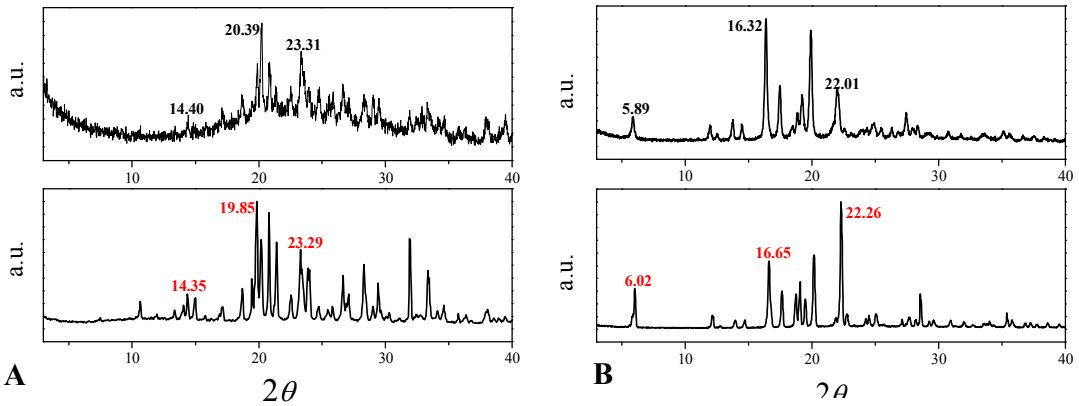

Figure 3: Powder X-ray patterns of milled (up) and non-milled (down). A) A-FMT and B) IBU.

As it is well known, amorphous solids must show not only the absence of diffraction peaks, but also the thermal signals inherent to these non-crystalline phases (i.e. T_g). Figure 4 displays IBU and A-FMT DSC curves as well as the obtained ones for 1:1 and 7:3 FMT-IBU binary systems. IBU exhibits a sharp melting endotherm at 74.4 ºC, while for A-FMT this event is observed at 165.86 ºC (Figure 4A). The DSC thermal curves of 1:1 and 7:3 FMT-IBU (Figures 4B and 4C, respectively) evidence a different thermal behavior in comparison to the pure APIs. T_gs at 45.46 ºC and 37.65 ºC were determined for 1:1 and 7:3 FMT-IBU, respectively, whereas this event occurs at -49 ºC in IBU and 76 ºC in FMT. Moreover, these CAMs show an exothermic event at ~ 85 ºC corresponding to the crystallization, followed by an endothermic process assigned to the melting of the now crystalline mixtures and almost immediate decomposition (Figure S2). This last event was the only one visualized by hot-stage microphotographs in both samples (Figures 4D and 4E). The occurrence of a single T_g, different enough from those of the isolated APIs, and the absence of diffraction peaks, confirm the formation of a homogeneous amorphous solid in both cases, where one component is dissolved in the other.[59] van Droogue *et al.*[60] suggest that the T_g value of a non interacting multicomponent system lies in the range between the T_gs of the isolated components, as it is observed for FMT-IBU CAMs.

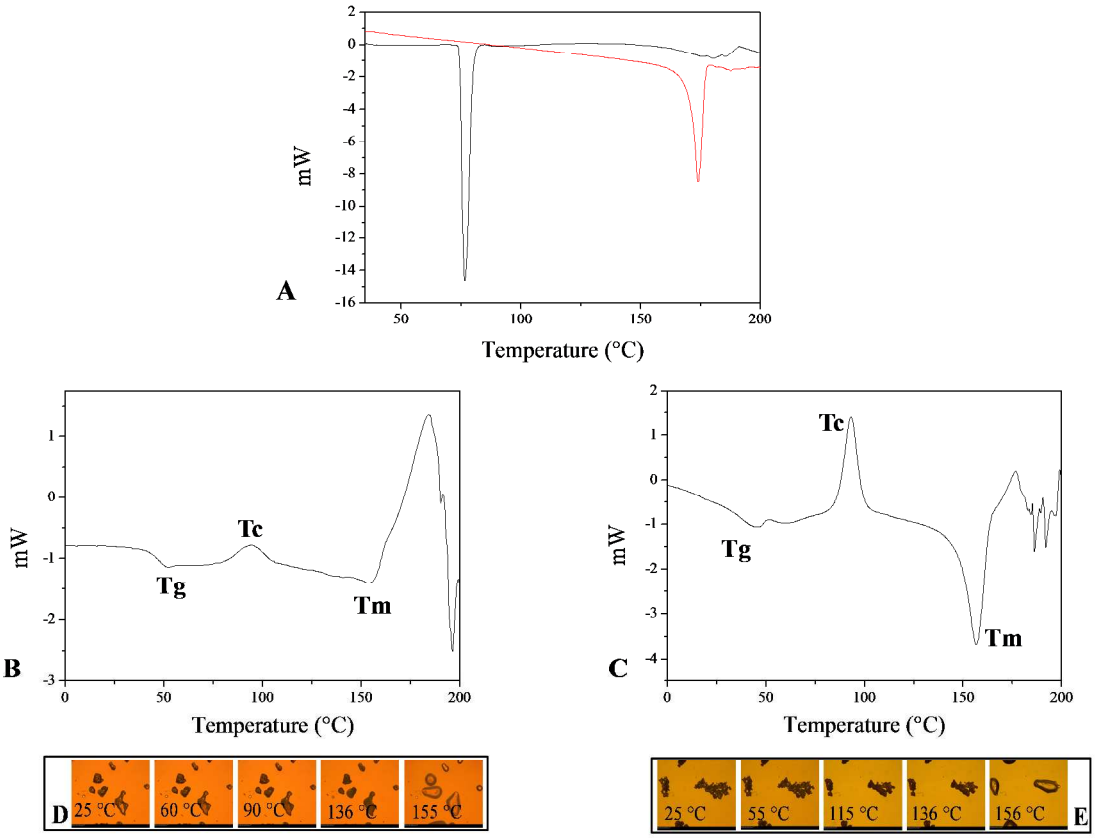

Figure 4: DSC curves of A) IBU (black) and A-FMT (red), B) 1:1 FMT-IBU and C) 7:3 FMT-IBU. Hot-stage microphotographs of D) 1:1 FMT-IBU and E) 7:3 FMT-IBU. (T_g: glass transition temperature; T_c: recrystallization temperature; T_m: melting temperature).

Beyond the previous considerations, it must be taken into account that the comparison of the T_g values experimental *vs.* those by the Gordon-Taylor equation (Equation 1) is also a powerful tool to determine the presence of intermolecular interactions in the CAM phases.[54] In this sense, similar values indicate that there are not intermolecular interactions in the CAM systems while different values suggest that the system components are intimately interacting. An experimental T_g value smaller than the calculated one can imply two possibilities: *i*: the intermolecular interactions are weaker compared to the pure amorphous components[61],[62] and *ii*: an increase in the APIs free volume due to grinding

process.[63] On the other hand, new and stronger intermolecular interactions in the CAMs than in the amorphous isolated components are present when the experimental T_g value is higher than the calculated one by the equation Gordon-Taylor equation.[64]

Table 1 shows the experimental and calculated T_g values corresponding to 1:1 and 7:3 FMT-IBU CAMs compared with those finding for pure amorphous FMT and IBU. Both FMT-IBU CAMs exhibit a positive deviation of the experimental T_g value with respect to the calculated ones according to the Gordon-Taylor equation. This fact evidences that FMT and IBU are intimately linked through intermolecular interactions; moreover, due to the greater deviation of the T_g value in 1:1 FMT-IBU, it is reasonable to assume that the strongest interactions are found in this system.

Table 1: Experimental and calculated T_g values for the amorphous isolated APIs, 1:1 and 7:3 FMT-IBU CAMs.

Sample	Experimental T_g (ºC)	Calculated T_g (ºC)
FMT	76	-
IBU	-49	-
1:1 FMT-IBU	45.46	10.9
7:3 FMT-IBU	37.65	36.33

It is convenient to remind that the glassy phase is unstable owing to its high energy and therefore, can recrystallize to an unwanted crystalline form. The evaluation of the physical stability of amorphous phases is performed by the storage of the samples in real time under different conditions of temperature and humidity during several periods.[65] In this work, the stability of the CAM was checked by XRPD and the obtained patterns are shown in Figure 5. The 7:3 FMT-IBU characteristic diffraction peaks belonging to crystalline A-FMT appear for all storage

temperatures, mainly in the assay at 40 °C (Figure 5A). On the other hand, in the 1:1 binary system no typical signals of crystalline drugs were observed (Figure 5B). This high physical stability and its higher T_g value, compared to the 7:3 FMT-IBU, denote stronger FMT-IBU interactions.

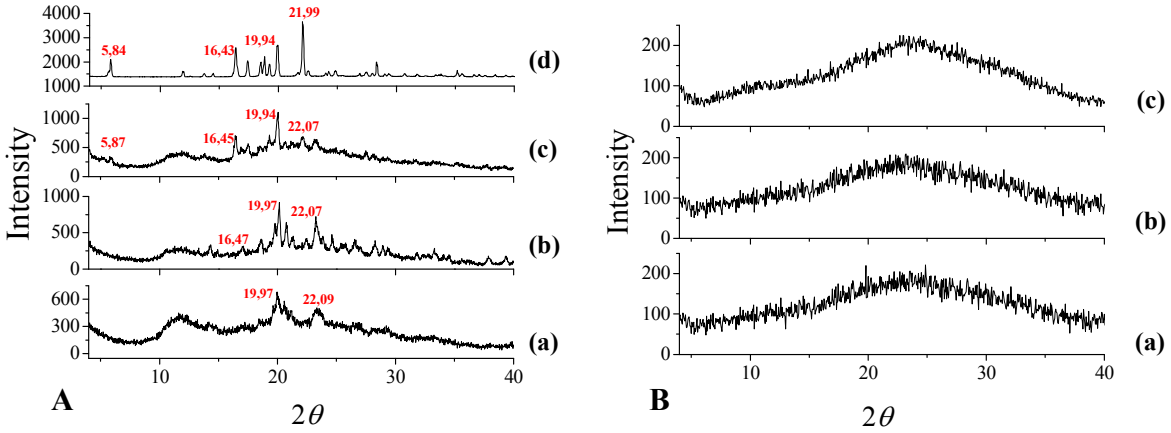

Figure 5: XRPD patterns after 60 days at different storage temperatures. A) 7:3 FMT-IBU at a: 4 ºC, b: 25 ºC and c: 40 ºC (The XRPD diagram corresponding to A-FMT is shown in Figure 5Ad); B) 1:1 FMT-IBU at a: 4 ºC, b: 25 ºC and c: 40 ºC.

For the amorphous state, the T_g-50 rule establishes that glass phases are physically stable when samples are stored at 50 °C below their corresponding T_g.[66] However, 1:1 FMT-IBU is stable to the three tested temperatures, none of them 50 ºC lower than its T_g value. Therefore, this system is an exception of the T_g-50 rule as it was found for other CAMs previously reported.[53] This fact suggests that there are different factors that affect the stability of amorphous phases like intermolecular interactions.

Taking into account that the intermolecular interactions are the main stabilizing factor in CAMs,[35] FTIR analysis was carried out to determine them. Figure 6 shows the FTIR spectra of both pure A-FMT and IBU in comparison with the corresponding to the 1:1 FMT-IBU, while the selected vibrational modes are listed in Table S1. Due to the FTIR

spectra complexity, the analysis is focused in those functional groups which could potentially participate in intermolecular interactions.

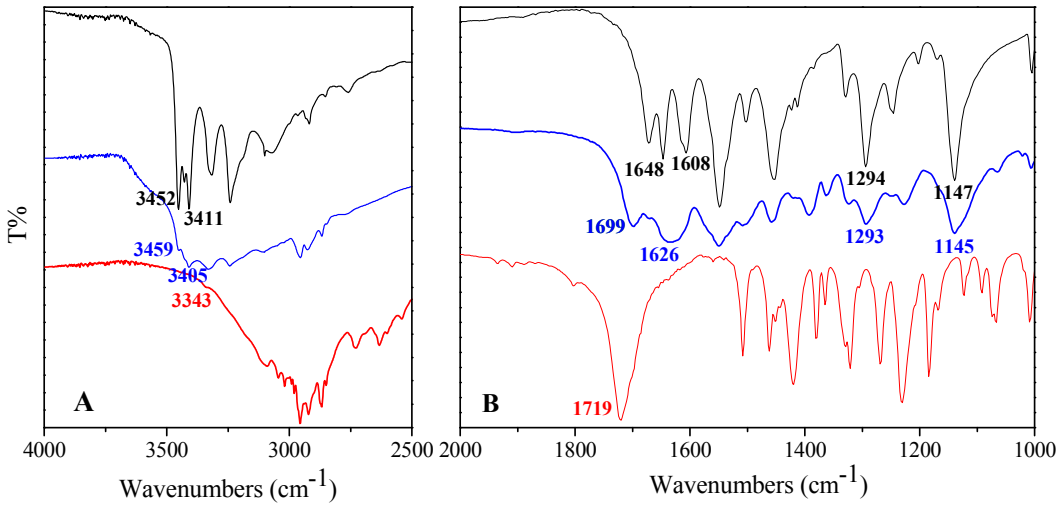

Figure 6: FTIR spectrum of IBU (red), A-FMT (black) and 1:1 FMT-IBU CAM (blue).

IBU shows the vibrational modes of the carboxylic group at 3343 and 1719 cm^{-1} which are assigned to $\nu(O_1\text{-}H)$ and $\nu(C_1{=}O_2)$, respectively. On the other hand, two centered sharp bands at 3452 and 3411 cm^{-1} corresponding to $\nu(N_{(1\text{ or }2)}\text{-}H)_{gua}$ moiety are visualized in the A-FMT spectrum, while the bands at 1648 and 1608 cm^{-1} are consistent with $\nu(C_{(1)}{=}N_{(3)})_{gua}$ and $\delta(N_{(1\text{ or }2)}\text{-}H)_{gua}$, respectively. Moreover, the vibrational modes of the sulfoxide group are observed at 1294 and 1147 cm^{-1} derived from to $\nu_{as}(S_1{=}O_{(1\text{ and }2)})$ y $\nu_{sym}(S_1{=}O_{(1\text{ and }2)})$, respectively.

The FTIR spectrum of 1:1 FMT-IBU shows broader bands in comparison with pure drugs; this fact strongly suggests modifications in the chemical environment after amorphization process.[67] Moreover, several shifts in the frequency values are observed in this sample regarding to the isolated APIs. In this sense, the $\nu(C_1{=}O_2)$ of IBU is shifted to a lower wavenumber (~ 20 cm^{-1}), while the $\nu(O_1\text{-}H)$ could not be assigned due to the overlapping

with FMT bands. No bands corresponding to the -COO^- group were observed indicating that no proton transfer between FMT and IBU occurs.

The vibrational modes of the guanidine moiety in the CAM 1:1 FMT-IBU strongly evidence the presence of intermolecular interactions when compared with those observed in A-FMT. The $\nu(N_{(1\ or\ 2)}\text{-}H)_{gua}$ shifts from 3452 – 3411 to 3459 - 3405 cm^{-1}, while the bands at 1648 and 1608 cm^{-1} assigned to $\nu(C_1{=}N_3)_{gua}$ and $\delta(N_{(1\ or\ 2)}\text{-}H)_{gua}$, respectively, appear as a unique band at 1626 cm^{-1} derived from the overlapping of both previous mentioned modes. The displacement to a lower frequency of the $\nu(C_1{=}N_3)_{gua}$ in 1:1 FMT-IBU CAMs indicates the weakening of this bond. The appearance to a higher frequency of the $\delta(N_{(1\ or\ 2)}\text{-}H)_{gua}$ represents a spectroscopic evidence of H-bond intermolecular interactions of greater strength with respect to A-FMT. In fact, the heterosynthon N-H⋯O is energetically more favored than the N-H⋯N one that is present in A-FMT.[33,68] The modes corresponding to $\nu_{as}(S_1{=}O_{(1\ and\ 2)})$ and $\nu_{sym}(S_1{=}O_{(1\ and\ 2)})$ do not show significant displacements in comparison with the API thus, any asseveration about new intermolecular interactions involving the sulfoxide group would be inconclusive.

The vibrational behavior of 1:1 FMT-IBU CAMs supports the interaction between FMT and IBU through the guanidine and carboxylic moieties, respectively, with possible formation of the heterosynthon displayed in Figure 1B. Then, the spectroscopic analysis is consistent with the positive deviation of the experimental T_g *vs.* the calculated (see Table 1) evidencing intermolecular interactions with such strength that allow us to justify the high stability of the present CAMs.

3.2. DFT calculations and Molecular dynamics (MD) simulations

3.2.1. Geometric optimization

In spite of the amorphous systems are characterized by the absence of long-range order, they have varying degrees of short-range order by H-bond interactions forming dimers or trimers. These arrangements improve physical stability and pharmacokinetic properties such as solubility and intrinsic dissolution rate of APIs in co-amorphous phases.[10] Taking into account the experimental data discussed in this paper, the high physical stability of 1:1 FMT-IBU can be attributed to intermolecular interactions through heterosynthon formation as shown in Figure 1B. In order to analyze the intermolecular interactions demonstrated by FTIR spectroscopy between FMT and IBU, *ab initio* calculations followed by QTAIM analysis were performed.

Crystallographic studies performed by Overgaard, J. *et al.*[33] and Shanklan, N. *et al.*[34] on FMT and IBU, respectively, were used to geometrical optimizations. Close agreement were found in distances and bond angles when comparing crystallographic *vs*. DFT results (Table S2). However, expected differences were observed in dihedral angles probably due to the low energy involved in the torsional changes after crystallographic packing relax (i.e. simple bonds rotations).[69] The optimized structures were employed to built the heterodimer FMT-IBU.

Figure 7 presents both conformers (A and B) designed to perform DFT calculation. The interaction between the guanidine group of FMT and the carboxilic group belonging to IBU, evidenced by FTIR spectroscopy, is present in the conformers. IBU shows a different spacial arrangement in the conformer A respect to the B one, about the dihedral angle O_2-C_1-C_2-C_4 whose rotation probably takes place during the milling process.[69] The geometrical

optimization reveals the conformer A as the minimun energy structure, thus such conformer was selected to perform QTAIM analysis.

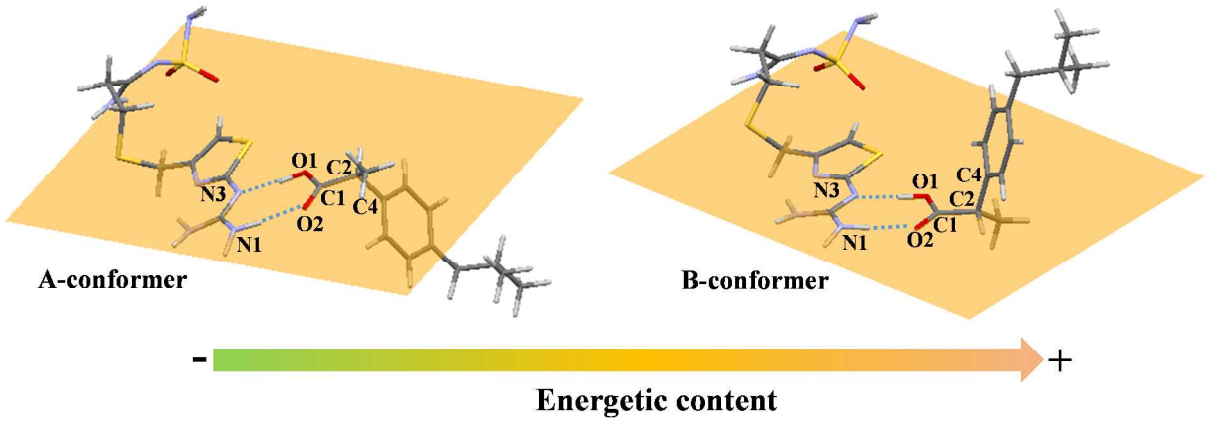

Figure 7: FMT-IBU conformers designed to quantum mechanical optimization. (The proposed intermolecular interaction is shown in the orange plane).

3.2.2. Topological analysis of the electron density

QTAIM allows the detailed analysis of the electron density distribution calculated by the quantum mechanical wavefunction or the quantum mechanical models refined from X-ray diffraction data. The Koch and Popelier electronic criteria[70] used in this paper were the charge density (ρ) and the Laplacian of the charge density ($\nabla^2\rho$). Molecular graph of conformer A is shown in Figure 8 and the bond critical points (BCPs) properties are listed in Table 2.

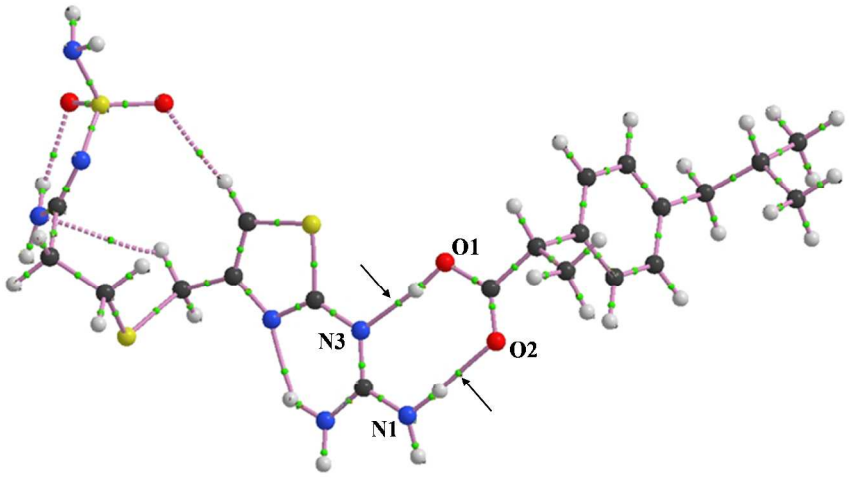

Figure 8: Molecular graph of A conformer showing the BCP (green points) and bond paths (purple line).

Table 2: Geometrical and topological parameters of intermolecular H-bonds found in the A conformer.

D-H···A	D-H[a] [Å]	D···A [Å]	H···A [Å]	D-H···A[°]	P	$\nabla^2\rho$
$O_{1(IBU)}$-H···$N_{3(FMT)}$	1.015	2.722	1.712	172.24	0.052648	0.097065
$N_{1(FMT)}$-H···$O_{2(IBU)}$	1.023	2.875	1.853	175.33	0.031306	0.107041

D: donor; A: acceptor

ρ: charge density: $\nabla^2\rho$: Laplacian of the charge density

Regarding to the Koch and Popelier criteria, BCPs and bond paths between FMT and IBU, involving the guanidine and carboxylic groups, respectively, were found (Figure 8, bold arrows). The strength and nature of these intermolecular interactions must be evaluated by analyzing the topological parameters in the BCPs. According to these authors, the numerical analysis of ρ and $\nabla^2\rho$ in a BCP denotes the strength of interaction, the corresponding values being between 0.002 – 0.034 u.a. and 0.024 – 0.139 u.a., respectively. The ρ values listed in Table 2 for the proposed conformer are found upper limit in $O_{1(IBU)}$-H···$N_{3(FMT)}$ whereas the $N_{1(FMT)}$-H···$O_{2(IBU)}$ interaction takes a high value. This fact

expresses the elevated strength of both intermolecular interactions, $O_{1(IBU)}$-H···$N_{3(FMT)}$ being the stronger one. Moreover, the calculated geometrical parameters are in agreement with this ρ value since the D···A and H···A distances are shorter in such interaction.

This analysis also supports the presence of strong intermolecular interactions involving the guanidine group of FMT and the carboxylic one from IBU as responsable of the high physical stability of 1:1 FMT-IBU and the positive deviation between experimental and calculated T_g values (Table 1).

3.2.3. Molecular Dynamic Simulations

MD simulations have been used in amorphous systems to study their dynamic parameters, structural properties[71] as well as to predict T_g.[72] In this sense, MD simulations were carried out to evaluate the FMT-IBU heterodimer formation through the intermolecular interactions proposed in Figure 1B.

With the purpose to determine the analogy between the proposed CAM assembly and the system prepared by co-milling, the T_g for the first system was obtained and further compared with the experimental one. For the co-amorphous assemble, the T_g is obtained by MD simulations graphing the change of density as a function of temperature;[71] the simulated value of the T_g is taken as the intersection point between the straights fitting up and below the transition. Linear sections of the corresponding density *vs.* temperature curve were identified by means of the lack-of-fit analysis employing the F-test with a $p < 0.05$ for the fits of linear data and starting at 150 or 380 K (Figure 9).

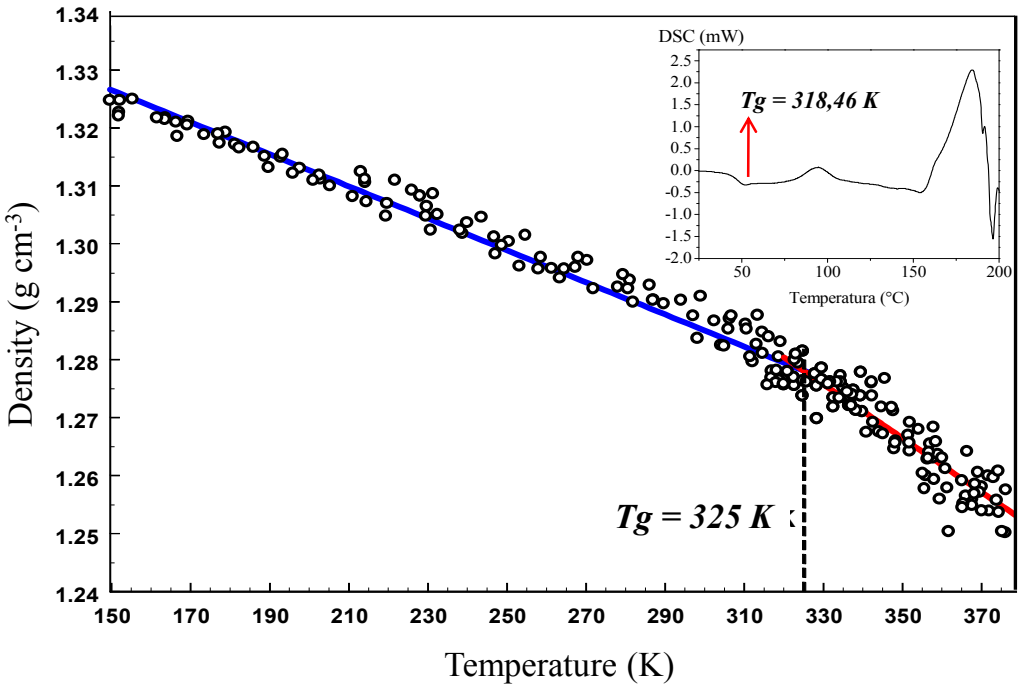

Figure 9: Density - temperature phase diagram of the simulated amorphous assembly. The system was cooled from 380 to 150 K at a 0.03 K ps^{-1} rate. The inset shows the DSC curve indicating the experimental T_g for the system obtained by co-milling.

The T_g value for a given system varies depending on the method by such amorphous material was prepared.[72] Even though, the 1:1 FMT-IBU was prepared by co-milling whereas quench-cooling (simulated annealing procedure) was employed to simulate the corresponding amorphous assembly, both Tg values (experimental and simulated), are in good agreement. From these results, it can be assumed that the proposed assembly for FMT-IBU closely reproduces the vitreous phase experimentally prepared.

In order to identify the probability of finding the proposed heterodimer in the simulated amorphous assembly the Radial Distribution Function (RDF) was analyzed.

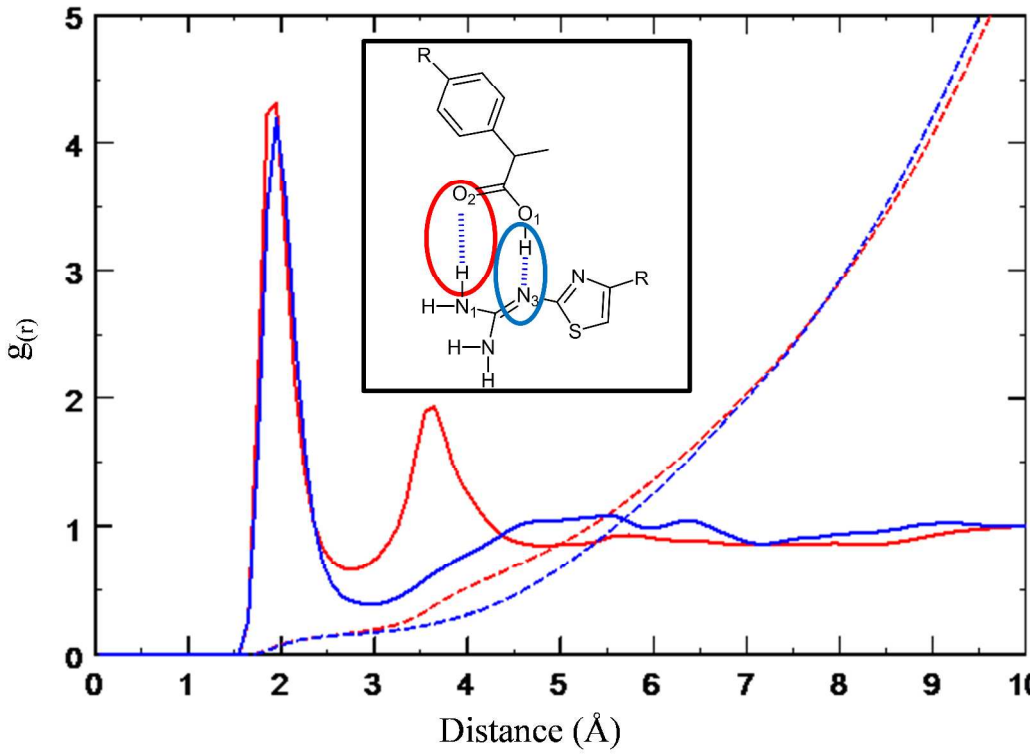

Figure 10: RDF curve between the O_2 (IBU) and the -N_1H (FMT) (blue) and the N_3 (FMT) and -O_1H (IBU) (red). The corresponding profiles derivatives are shown in dash lines.

The RDF profile at 298 K for the amorphous assembly is shown in Figure 10 where only the atoms involved in those interactions proposed in Figure 1B, are displayed. Two sharp peaks can be observed for $O_{2(IBU)}\cdots H_{(FMT)}$ and $N_{3(FMT)}\cdots H_{(IBU)}$ pairs at 1.75 and 1.88 Å, respectively; these results are clearly consistent with the presence of such proposed FMT and IBU intermolecular interactions. The values obtained by RDF for the corresponding interatomic distances fit well with those calculated by DFT geometrical optimization (Table 2), indicating that the geometry and strength of the interactions analyzed by QTAIM are maintained in the proposed thermodynamic amorphous assembly.

RDF analysis confirms the intermolecular interactions N_3-H$\cdots O_1$ and O_2-H$\cdots$N1, however, the presence of the heterodimers formed *via* these interactions, that give rise to eight-

members rings ($R_2^2 8$), could not be demonstrated. Therefore, a manual searching inside the proposed amorphous phase was performed with the aim to identify such species. Figure 11 (A-D) displays the obtained results where such H-bonding motifs are present. In addition to these interactions, FMT and IBU are also forming heterodimers $R_2^2 8$ based in a N-H···O heterosynthon involving the amino groups of the guanidine moiety (FMT) as H-donors and the IBU carboxylic one (Figure S3 A-B). Moreover, interactions between the amino group belonging to the sulfamoyl moiety (FMT) and the IBU carboxylic one were also found (Figure S3 C). Chain-type interactions determining trimers and H-bonds between the guanidine moiety and the IBU hydroxyl group ($N_{3(FMT)}$···H-$O_{1(IBU)}$) could be observed too (Figure S3 D and E, respectively). No evidences of intermolecular interactions involving the O atoms of the sulfamoyl group as H-bond acceptors were found, consistent with the FTIR experimental data. It is worth mentioning that the variety of H-bonds found in the simulated amorphous assembly, allows us to justify the broadening of the bands in the FTIR spectrum of 1:1 FMT-IBU since a same functional group is present in different chemical environments.

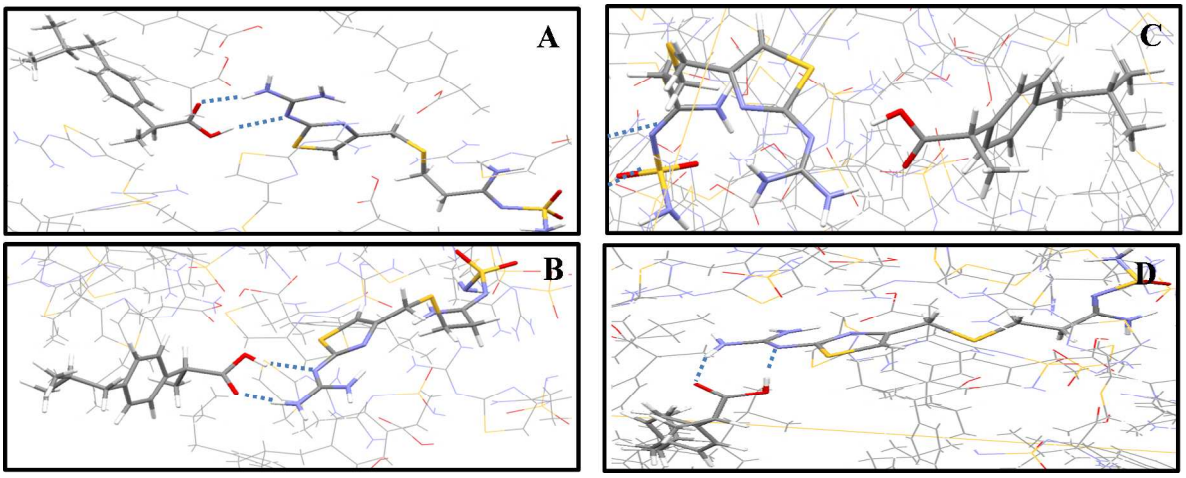

Figure 11: Significant H-bond interactions found in the simulated amorphous assembly.

4. CONCLUSIONS

Famotidine and ibuprofen were selected as models drugs to obtain a co-amorphous system through the co-milling technique, rationally designed for stabilizing by formation of heterodimers between both drugs. Three binary systems in 3:7, 1:1 and 7:3 molar ratios of A-FMT and IBU, respectively, were prepared; the latter ones were completely converted into the amorphous state after 180 minutes of co-milling. Contrarily, no amorphous solids were obtained when the same mechanical process was applied separately to A-FMT and IBU. This fact confirms that the crystalline order of each drug is easier to disorganize when both drugs are milled together, associated to the formation of more stable intermolecular interactions. The stability assays evidenced the poor physical stability of the 7:3 FMT-IBU whereas the corresponding 1:1 system retains its amorphous nature under the tested conditions, suggesting the presence of strong intermolecular interactions that prevent re-crystallization of the isolated drugs. In this sense, $N_{3(FMT)}\cdots H\text{-}O_{1(IBU)}$ and $N_1\text{-}H_{(FMT)}\cdots O_{2(IBU)}$ H-bonds were particularly assessed as those able to form a $R_2^2 8$ structural motif. The formation of the expected intermolecular interactions was supported by modifications of the 1:1 FMT-IBU FTIR spectrum in comparison with those of the pure APIs. DFT calculations allowed us to select the minimum energy heterodimer; further QTAIM analysis suggests a high strength of the proposed interactions. MD simulations along with a simulated annealing procedure were employed to construct a thermodynamic amorphous assembly that resulted in an adequate and realistic representation of the experimentally obtained vitreous phase, according to the close T_gs values (simulated and experimental). RDF curves account for the expected intermolecular interactions but not the

formation of the $R_2^2 8$ motif, which could be detected performing a manual searching into the simulated amorphous assemble. In summary, this work proposes that a co-amorphous binary system, physically stable, could be rationally designed by selecting components without other competitive interactions, able to prevent the desired structural motif.

AUTHOR INFORMATION

Corresponding Author

*(Telephone: +54 (0266) 4520300 (Int. 6117); e-mail: mgrusso@unsl.edu.ar, gnarda@unsl.edu.ar

ASSOCIATED CONTENT

Supplementary Information

The Supplementary Information are available free of charge. DSC curves from -30 to 200 °C of A) 1:1 FMT-IBU and B) 7:3 FMT-IBU (Figure S1). DSC and TG curves of A) 1:1 FMT-IBU and B) 7:3 FMT-IBU (Figure S2). Selected vibrational modes of IBU, A-FMT and 1:1 FMT-IBU (Table S1). Crystallographic and DFT data of A-FMT and IBU (Table S2). Significant H-bond interactions found in the simulated amorphous assembly (Figure S3).

ACKNOWLEDGMENT

Financial support from Universidad Nacional de San Luis, Argentina (Proico 2-2016) is gratefully acknowledged. MGR thanks Consejo Nacional de Investigaciones Científicas y Técnicas (CONICET) for a fellowship and financial support (PIP CONICET 112-201101-00912).

REFERENCES

(1) Grohganz, H.; Priemel, P. A.; Löbmann, K.; Nielsen, L. H.; Laitinen, R.; Mullertz, A.; Van den Mooter, G.; Rades, T. Refining Stability and Dissolution Rate of Amorphous Drug Formulations. *Expert Opin. Drug Deliv.* **2014**, *11,* 977–989.

(2) Rumondor, A. C. F.; Dhareswar, S. S.; Kesisoglou, F. Amorphous Solid Dispersions or Prodrugs: Complementary Strategies to Increase Drug Absorption. *J. Pharm. Sci.* **2016**, *105*, 2498-2508.

(3) Du, J. D.; Hong, L.; Tan, A.; Boyd, B. J. Naphthlocyanine as New Photothermal Actuator for Lipid-based Drug Delivery Systems. *J. Phys. Chem.* B. **2018**, *122*, 1766-1770.

(4) Russo, M. G.; Brusau, E. V.; Ellena, J.; Narda, G. E. Solid-state Supramolecular Synthesis Based on the N-H···O Heterosynthon: An Approach to Solve the Polymorphism Problem in Famotidine. *J. Pharm. Sci.* **2014**, *103*, 3754–3763.

(5) Surov, A. O.; Volkova, T. V.; Churakov, A. V.; Proshin, A. N.; Terekhova, I.V.; Perlovich, G. L. Cocrystal Formation, Crystal Structure, Solubility and Permeability Studies for Novel 1,2,4-thiadiazole Derivative as a Potent Neuroprotector. *Eur. J. Pharm. Sci.* **2017**, *109*, 31-39.

(6) Tricarico, D.; Maqoud, F.; Curci, A.; Camerino, G.; Zizzo, N.; Denora, N.; Cutrignelli, A.; Laquintana, V.; Lopalco, A.; la Forgia, F. et al. Characterization of Minoxidil/Hydroxypropyl-β-cyclodextrin Inclusion Complex in Aqueous Alginate Gel Useful for Alopecia Management: Efficacy Evaluation in Male Rat. *Eur. J. Pharm. and Biopharm.* **2018**, *122*, 146 – 157.

(7) de Sousa Marcial, S. P.; Carneiro, G., Leite, E. A. Lipid-Based Nanoparticles as Drug Delivery System for Paclitaxel in Breast Cancer Treatment. *J. Nanoparticle Res.* **2017**, *19,* 340-351.

(8) Amstad, E.; Spaepen, F., Weitz, D. A. Stabilization of the Amorphous Structure of Spray-Dried Drug Nanoparticles. *Chem. Phys. B.* **2016**, *120*, 9161-9165.

(9) Ogawa, N.; Hiramatsu, T.; Suzuki, R.; Okamoto, R.; Shibagaki, K.; Fujita, K.; Takahashi, C.; Kawashima, Y.; Hiromitsu, Y. Improvement in the Water Solubility of Drugs with a Solid Dispersion System by Spray Drying and Hot-melt Extrusion with Using the Amphiphilic Polyvinyl Caprolactam-Polyvinyl Acetate-Polyethylene Glycol Graft Copolymer and d-mannitol. *Eur. J. Pharm. Sci*. **2018**, *111*, 205–214.

(10) Löbmann, K.; Strachan, C.; Grohganz, H.; Rades, T.; Korhonen, O.; Laitinen, R. Co-amorphous Simvastatin and Glipizide Combinations Show Improved Physical Stability Without Evidence of Intermolecular Interactions. *Eur. J. Pharm. Biopharm.* **2012**, *81,* 159-169.

(11) Laitinen, R.; Löbmann, K.; Strachan, C. J.; Grohganz, H.; Rades, T. Emerging Trends in the Stabilization of Amorphous Drugs. *Int. J. Pharm.* **2013**, *453*, 65–79

(12) Forster, A.; Hempenstall, J.; Rades, T. Characterization of Glass Solutions of Poorly Water-Soluble Drugs Produced by Melt Extrusion with Hydrophilic Amorphous Polymers. *J. Pharm. Pharmacol*. **2001**, *53*, 303–315.

(13) Moinuddin, S. M.; Ruan, S.; Huang, Y.; Gao, Q.; Shi, Q.; Cai, B.; Cai, T. Facile Formation of Co-amorphous Atenolol and Hydrochlorothiazide Mixtures Via Cryogenic-milling: Enhanced Physical Stability, Dissolution and Pharmacokinetic Profile. *Int. J. Pharm.* **2017**, *532*, 393–400.

(14) Ueda, H.; Kadota, K.; Imono, M.; Ito, T.; Kunita, A.; Tozuka, Y.; Co-amorphous Formation Induced by Combination of Tranilast and Diphenhydramine Hydrochloride. *J. Pharm. Sci.* **2017**, *106*, 123– 28.

(15) Dengale, S. J.; Hussen, S. S.; Krishna, B. S. M.; Musmade, P.; Gautham Shenoy, G.; Bhat, K. Fabrication, Solid State Characterization and Bioavailability Assessment of Stable Binary Amorphous Phases of Ritonavir with Quercetin. *Eur. J. Pharm. Biopharm.* **2015**, *89*, 329–338.

(16) Wu, W.; Löbmann, K.; Rades, T.; Grohganz, H. On the Role of Salt Formation and Structural Similarity of Co-formers in Co-amorphous Drug Delivery Systems. *Int. J. Pharm.* **2018**, *535,* 86–94.

(17) Ojarinta, R.; Lerminiaux, L.; Laitinen, R. Spray Drying of Poorly Soluble Drugs From Aqueous Arginine Solution. *Int. J. Pharm.* **2017**, *532*, 289–298.

(18) Ojarinta, R.; Heikkinen, A. T.; Sievänen, E.; Laitinen, R. Dissolution Behavior of Co-amorphous Amino Acid-Indomethacin Mixtures: The Ability of Amino Acids to Stabilize the Supersaturated State of Indomethacin. *Eur. J. Pharm. Biopharm*. **2017**, *112,* 85–95.

(19) Huang, Y.; Zhang, Q.; Wang, J. R.; Lin, K. L.; Mei, X. Amino Acids as Co-amorphous Excipients for Tackling the Poor Aqueous Solubility of Valsartan. *Pharm. Dev. Technol.* **2017**, *22,* 69–76.

(20) Löbmann, K.; Grohganz, H.; Laitinen, R.; Strachan, C.; Rades, T. Amino Acids as Co-amorphous Stabilizers for Poorly Water Soluble Drugs Part 1: Preparation, Stability and Dissolution Enhancement. *Eur. J. Pharm. Biopharm.* **2013**, *85*, 873–881.

(21) Löbmann, K.; Laitinen, R.; Strachan, C.; Rades, T.; Grohganz, H. Amino Acids as Co-amorphous Stabilizers for Poorly Water-Soluble Drugs Part 2: Molecular Interactions. *Eur. J. Pharm. Biopharm.* **2013**, *85,* 882–888.

(22) Korhonen, O.; Pajula, K.; Laitinen, R. Rational Excipient Selection for Co-amorphous Formulations. *Expert Opin. Drug Deliv*. **2017**, *14*, 551–569.

(23) Löbmann, L.; Laitinen, R.; Grohganz, H.; Gordon, K. C.; Strachan, C.; Rades, T. Co-amorphous Drug Systems: Enhanced Physical Stability and Dissolution Rate of Indomethacin and Naproxen. *Mol. Pharmaceutics* **2011**, *8*, 1919–1928.

(24) Löbmann, K.; Laitinen, R.; Grohganz, H.; Strachan, C.; Rades, T.; Gordon, K. C. A Theoretical and Spectroscopic Study of Co-amorphous Naproxen and Indomethacin. *Int. J. Pharm.* **2013**, *453,* 80-87.

(25) Dengale, S. J.; Hussen, S. S.; Krishna, B. S. M.; Musmade, P. B.; Gautam Shenoy, G. G.; Bhat, K. Fabrication, Solid State Characterization and Bioavailability Assessment of Stable Binary Amorphous Phases of Ritonavir with Quercetin. *Eur. J. Pharm. Biopharm*. **2015**, *89,* 329-338.

(26) Etter, M. C. Encoding and Decoding Hydrogen-Bond Patterns of Organic Compounds. *Acc. Chem. Res.* **1990**, *23*, 120-126.

(27) Etter, M. C. Hydrogen Bonds as Design Elements in Organic Chemistry. *Phys. Chem.* 1991, *95*, 4601-4609.

(28) Button, R. G.; Cairns, J. P.; Taylor, P. J. Tautomeric Ratio in 4-methylthiazol-2-ylguanidine, a Model Guanidinoheterocycle. *J. Chem. Soc. Perkin. Trans.* **1985**, *2,* 1555–1558.

(29) Olea-Azar, C.; Parra-Mouchet, J. Conformational Studies on 2-guanidinylthiazole, Famotidine and Some Analogues. *J. Mol. Struct. (THEOCHEM)*. **1997**, *390*, 239–245.

(30) Steiner, T. The Hydrogen Bond in the Solid State. *Angew. Chem. Int. Ed.* **2002**, *41,* 48-76.

(31) Hassan, M. A; Salem, M. S.; Sueliman, M. S.; Najib, N. M. Characterization of Famotidine Polymorphic Forms. *Int. J. Pharm*. **1997**, *149*, 227–232.

(32) Lu, J.; Wang, X. J.; Yang, X.; Ching, C. B. Polymorphism and Crystallization of Famotidine. *Cryst. Growth Des*. **2007**, *7*, 1590-1598.

(33) Overgaard, J.; Hibbs, D. E. The Experimental Electron Density in Polymorphs A and B of the Anti-Ulcer Drug Famotidine. *Acta Crystallogr. Sect. A*. **2004**, *60*, 480-487.

(34) Shankland, N.; Wilson, C. C.; Florence, A. J.; Cox, P. J. Refinement of Ibuprofen at 100 K by Single-Crystal Pulsed Neutron Diffraction. *Acta Crystallogr*. **1997**, *C53*, 951-954.

(35) Alleso, M.; Chieng, N.; Rehder, S.; Rantanen, J.; Rades, T.; Aaltonen, J. Enhanced Dissolution Rate and Synchronized Release of Drugs in Binary Systems Through Formulation: Amorphous Naproxen-Cimetidine Mixtures Prepared by Mechanical Activation. *J. Control. Rel.* **2009**, *136*, 45-53.

(36) Hancock, B. C.; Carlson, G. T.; Ladipo, D. D.; Langdon, B. A.; Mullarney, M. P. Comparison of the Mechanical Properties of the Crystalline and Amorphous Forms of a Drug Substance. *Int. J. Pharm.* **2002**, *241*, 73-85.

(37) Rehman, M.; Shekunov, B. Y.; York, P.; Lechuga-Ballesteros, D.; Miller, D. P.; Tan, T.; Colthorpe, P. Optimization of Powders for Pulmonary Delivery Using Supercritical Fluid Technology. *Eur. J. Pharm. Sci.* **2004**, *22*, 1-17.

(38) Frisch, M. J.; Trucks, G. W.; Schlegel, H. B.; Scuseria, G. E.; Robb, M. A.; Cheeseman, J. R.; Scalmani, G.; Barone, V.; Mennucci, B.; Petersson, G. A. et al. Gaussian 09, Revision A.2; Gaussian, Inc.: Wallingford, CT, 2016.

(39) Becke, A. D. Density-Functional Thermochemistry. III. The Role of Exact Exchange. *J. Chem. Phys.* **1993**, *98*, 5648-5652.

(40) Ditchfield, R.; Hehre, W. J.; Pople, J. A. Self-Consistent Molecular-Orbital Methods. IX. An Extended Gaussian-Type Basis for Molecular-Orbital Studies of Organic Molecules. *J. Chem. Phys.* **1971**, *54*, 724–728.

(41) Bader, R. F. W. Atoms in Molecules: A Quantum Theory, Oxford University Press, Oxford, **1990**.

(42) AIMPAC, http://www.chemistry.mcmaster.ca/aimpac. (accessed 20 July, 2018)

(43) Case, D. A.; Cerutti, D. S.; Cheatham, T. E., Darden, F.; Cheatham, R. E.; Duke, T. J.; Giese, H.; Gohlke, A. W.; Goetz, D.; Greene, N. et al. AMBER, University of California, San Francisco., 2017.

(44) Wang, J.; Wolf, R. M.; Caldwell, J. W.; Kollamn, P. A.; Case, D. A. Development and Testing of a General Amber Force Field. *J. Comput. Chem.* **2004**, *25*, 1157–1174.

(45) Salomon-Ferrer, R.; Goetz, A. W.; Poole, D.; Le Grand, S.; Walker, R. C. Routine Microsecond Molecular Dynamics Simulations with AMBER - Part II: Particle Mesh Ewald. *J. Chem. Theory Comput.* **2013**, *9*, 3878-3888.

(46) Rehman, M.; Shekunov, B. Y.; York, P.; Lechuga-Ballesteros, D.; Miller, D. P.; Tan, T.; Colthorpe, P. Optimization of Powders for Pulmonary Delivery Using Supercritical Fluid Technology. *Eur. J. Pharm. Sci.* **2004**, *22*, 1-17.

(47) Le Grand, S.; Goetz, A. W.; Walker, R. C. SPFP: Speed Without Compromise a Mixed Precision Model for GPU Accelerated Molecular Dynamics Simulations. *Comp. Phys. Comm.* **2013**, *184*, 374-380.

(48) Case, D. A.; Betz, R. M.; Cerutti, D. S.; Cheatham, T. E.; Darden, T. A.; Duke, R. E.; Giese, T. J.; Gohlke, H.; Goetz, A. W.; Homeyer, N.; Izadi, S. et al. AMBER University of California, San Francisco, 2016.

(49) Cerutti, D. S.; Duke, R. E.; Darden, T. A.; Lybrand, T. P. Staggered Mesh Ewald: An Extension of the Smooth Particle-Mesh Ewald Method Adding Great Versatility. *J. Chem. Theory Computat.* **2009**, *5*, 2322–2338.

(50) Miyamoto, S.; Kollman, P. A. SETTLE: An Analytical Version of the SHAKE and RATTLE Algorithm for Rigid Water Models. *J. Comput. Chem.* **1992**, *13*, 952–962.

(51) Izaguirre, J. A.; Catarello, D. P.; Wozniak, J. M.; Skeel, R. D. Langevin Stabilization of Molecular Dynamics. *J. Chem. Phys.* **2001**, *114*, 2090–2098.

(52) Berendsen, H. J. C.; Postma, J. P. M.; van Gunsteren, W. F.; Di Nola, A.; Haak, J. R. Molecular Dynamics with Coupling to an External Bath. *J. Chem. Phys.* **1984**, *81*, 3684-90.

(53) Perissuttia, B.; Passerinib, N.; Trastullob, R.; Keiserc, J.; Zanolla, D.; Zingonea, G.; Voinovicha, D.; Albertinib, B., *Int. J. Pharm.* **2017**, *532*, 402-412.

(54) Chieng, N.; Aaltonen, J.; Saville, D.; Rades, T. Physical Characterization and Stability of Amorphous Indomethacin and Ranitidine Hydrochloride Binary Systems Prepared by Mechanical Activation. *Eur. J. Pharm. Biopharm.* **2009**, *71*, 47–54.

(55) Dengale, S. J.; Ranjan, O. P.; Hussen, S. S.; Krishna, B. S. M.; Musmade, P. B., Gautham-Shenoy, G.; Bhat, K. Preparation and Characterization of Co-amorphous Ritonavir-Indomethacin Systems by Solvent Evaporation Technique: Improved Dissolution

Behavior and Physical Stability Without Evidence of Intermolecular Interactions. *Eur. J. Pharm. Sci.* **2014**, *62*, 57–64.

(56) Löbmann, K.; Strachan, C.; Grohganz, H.; Rades, T.; Korhonen, O.; Laitinen, R. Co-amorphous Simvastatin and Glipizide Combinations Show Improved Physical Stability Without Evidence of Intermolecular Interactions. *Eur. J. Pharm. Biopharm.* **2012**, *81,* 159-169.

(57) Qian, S.; Cheng, W.; Wei, Y.; Zhang, J.; Gao, Y. Coamorphous Lurasidone Hydrochloride–Saccharin with Charge-Assisted Hydrogen Bonding Interaction Shows Improved Physical Stability and Enhanced Dissolution with pH-Independent Solubility Behavior. *Cryst. Growth. Des*. **2015**, *15,* 2920-2928.

(58) Beyer, A.; Groganz, H.; Löbmann, K.; Rades, T.; Leopold, C. S. Influence of the Cooling Rate and the Blend Ratio on the Physical Stability of Co-amorphous Naproxen/Indomethacin. *Eur. J. Pharm. Biopharm.* **2016**, *109*, 140-148.

(59) Dengale, S. J.; Hussen, S. S.; Krshna, B. S. M.; Musmade, P. B.; Shenoy, G. G.; Bhat, K. Fabrication, Solid State Characterization and Bioavailability Assessment of Stable Binary Amorphous Phases of Ritonavir with Quercetin. *Eur. J. Pharm. Biopharm.* **2015**, 89, 329-338.

(60) van Droogue, D. J.; Hinrichs, W. L. J.; Visser, M. R.; Frijlink, H. W; Characterization of the Molecular Distribution of Drugs in Glassy Solid Dispersions at the Nano-meter Scale, Using Differential Scanning Calorimetry and Gravimetric Water Vapour Sorption Techniques. *Int. J. Pharmaceutics*. **2006**, *310*, 220-229.

(61) Nair, R.; Nyamweya, N.; Gönen, S.; Martinez-Miranda, L. J.; Hoag, S.W.; Influence of Various Drugs on the Glass Transition Temperature of Poly(vinylpyrrolidone): A Thermodynamic and Spectroscopic Investigation. *Int. J. Pharm.* **2001**, *225*, 83-96.

(62) Gupta, P.; Thilaqavathi, R.; Chakraborti, A. K.; Bansal, A. K. Role of Molecular Interaction in Stability of Celecoxib-PVP Amorphous Systems. *Mol. Pharm.* **2005**, *2,* 384-391.

(63) Shamblin, S. L.; Taylor, L. S.; Zografi, G. Mixing Behavior of Colyophilized Binary Systems. *J. Pharm. Sci.* **1998**, *87*, 694–701.

(64) Laitinen, R.; Löbmann, K.; Grohganz, H.; Strachan, C.; Rades, T. Amino Acids as Co-amorphous Excipients for Simvastatin and Glibenclamide: Physical Properties and Stability. *Mol. Pharmaceutics*. **2014**, *11*, 2381-2389.

(65) Grohganz, H.; Löbmann, K.; Priemel, P.; Tarp Jensen, K.; Graeser, K.; Strachan, C.; Rades, T. Amorphous Drugs and Dosage Forms. *J. Drug Deliv. Sci. Tech.* **2013**, *23*, 403-408.

(66) Hancock, B. C.; Shamblin, S. L.; Zografi, G. Molecular Mobility of Amorphous Pharmaceutical Solids Below Their Glass Transition Temperatures. *Pharm. Res.* **1995**, *12*, 799-806.

(67) Kaushal, A. M.; Chakraborti, A. K.; Bansal, A. K. FTIR Studies on Differential Intermolecular Association in Crystalline and Amorphous States of Structurally Related Non-Steroidal Anti-Inflammatory Drugs. *Mol. Pharm.* **2008**, *5*, 937-945.

(68) Adalder, T. K.; Sankolli, R.; Dastidar, P. Homo- or Heterosynthon? A Crystallographic Study on a Series of New Cocrystals Derived From Pyrazinecarboxamide

and Various Carboxilic Acids Equipped with Additional Hydrogen Bonding Sites. *Cryst. Growth Des.* **2012**, *12*, 2533-2542.

(69) Bernstein, J.; Hagler, A. T. Conformational Polymorphism. The Influence of Crystal Structure on Molecular Conformation. *J. Am. Chem. Soc.* **1978**, *100*, 673-681.

(70) Koch, U.; Popelier, P. L. A.; Characterization of C-H-O Hydrogen Bonds on the Basis of the Charge Density. *J. Phys. Chem.* **1995**, *99,* 9747–9754.

(71) Xiang, T. X.; Anderson, B. D. Molecular Dynamics Simulation of Amorphous Indomethacin. *Mol. Pharmaceutics* **2013**, *10*, 102-114.

(72) Gupta, J.; Nunes, C.; Jonnalagadda, S. A Molecular Dynamics Approach for Predicting the Glass Transition Temperature and Plasticization Effect in Amorphous Pharmaceuticals. *Mol. Pharmaceutics*, **2013**, *10*, 4136-4145

TOC Graphic